Penerbit Akademia Baru

Journal of Advanced Research in Materials Science
ISSN (online): 2289-7992 | Vol. 4, No.1. Pages 31-46, 2015

Three Dimensional Shoreline Changes Simulation Using Hybrid Genetic Algorithm of Interferometric Synthetic Aperture Radar

M. Marghany

Institute of Geospatial Science and Technology (INSTeG), Universiti Teknologi Malaysia
81310 UTM, Skudai, Johor Bahru, Malaysia
* *maged@utm.my, magedupm@hotmail.com*

Abstract – *The paper has demonstrated InSAR phase unwrapping using Hybrid Genetic Algorithm (GHA). The three dimensional phase unwrapping is performed using three-dimensional best-path avoiding singularity loops (3DBPASL) algorithm. Then phase matching is implemented with 3DBPASL using Hybrid Genetic Algorithm (GHA). Further, the combination between GHA and 3DBPASL is used to eliminate the phase decorrelation impact from the interferograms. The study shows that InSAR produces discontinues interferogram pattern because of the high decorelation. On the contrary, the three-dimensional sorting reliabilities algorithm generated 3-D coastline deformation with bias of -0.06 m, lower than ground measurements and the InSAR method. Therefore, 3DBPASL algorithm has a standard error of mean of ± 0.03 m, lower than ground measurements and the InSAR method. Consequently, the 3D-SRA is used to eliminate the phase decorrelation impact from the interferograms. The study also shows the performance of InSAR method using the combination of HGA and 3DBPASL is better than InSAR procedure which is validated by a lower range of error (0.04±0.22 m) with 90% confidence intervals. In conclusion, HGA algorithm can be used to solve the problem of decorrelation and produced accurate 3-D coastline deformation using ENVISAT ASAR data.*

Keywords: Hybrid Genetic Algorithm, Three-dimensional best-path avoiding singularity loops, Decorrelation, Interferogram, Coastal volume erosion

1.0 INTRODUCTION

Interferometric synthetic aperture radar (InSAR) techniques have excellent potentials to measure the millimeter-scale of the Earth‘s surface deformation. However, the main problem is raised in InSAR techniques is phase unwrapping. Therefore, phase unwrapping unwrapping is the procedure of repossessing clear-cut phase values from a 2-D array of phase known only modulo 2π radians. Indeed, phase unwrapping is a vital process to reconstruct three-dimensional object changes which is based on its digital elevation model (DEM). In this concern, digital elevation maps can be produced by implementing the single look complex synthetic aperture radar (SAR) images that are received by two or more separate antennas. The phase image is produced by multiplying the complex SAR image by the coregistered complex conjugate pixels of the other SAR data. Incidentally, the phase difference of the two SAR data is processed to acquire height and or deformation of the Earth’s surface. Consistent with, Zebker et al., [23] and Zhong et al., [43] the absolute value of the real phase difference

between any two neighboring pixels is less than π, then the real phase can be acquired by integrating the wrapped values of the wrapped phase differences. Neverthless, wrapped phase image is extremely challenged by several factors. Particulary, these critical factors are involved multiplactive speckle noises, shadow, foreshortening, layover, temporal, geometric and atmospheric decorrelations [1, 3, 15, 24, 31] which are negatively produced area of non-standard phase i.e. low quality area [29, 32, 43]. In this respect, low quality area can contribute to critical decorrelation issues in the phase unwrapping procedures.

Several phase unwrapping algorithms have been introduces to solve the cirtical issue of low quality area and the decorrelation. These algorithms are categorized into: (i) path-following algorithms and (ii) minimum-norm algorithms [44]. Subsequently, minimum-norm algorithms express the unwrapping issue in terms of minimization of the global function as compared to path-following algorithms. Conversely, the constraint of minimum-norm algorithms cannot be involved every individual pixels in the phase unwrapping procedures [43]. In contrast, path-following algorithms are extremely advanced compared to minimum-norm algorithms. The advances of path-following algorithms to: (i) identify the residues and uses the quality map to guide the generation of branch cuts by implementing branch cut [32] and mask cut algorithm [45]; (ii) to guide the path of integration which is function of quality-guided algorithm and (iii) to dismiss the total discontinuities of the unwrapped result by using minimum discontinuity algorithm [30, 37]. Besides, there are other phase unwrapping algorithms. Therefore, the conventional phases unwrapping region-growing and the least-square algorithms, which are required accurate image coregistration to be about 1/10 to 1,100 resolution cell size (i.e., SAR pixel [35]. In this context, Hai and Renbiao [5] stated that the interferometric phase unwrapping method which is based on subspace projection can provide an accurate estimation of the terrain interferometric phase (interferogram) even if the coregistration error reaches one pixel algorithms, such as the branch-cut method [12, 35],

Commonly, the accuracy of the image coregistertion is serious issue for accurate interferometric phase unwrapping. It is well known that the performance of interferometric phase unwrapping suffers seriously from poor image coregistration. Therefore, TanDEM-X and TerraSAR-X have been implemented to maintain the issue of image coregistration. Further, ERS-1 and ERS-2, Terara X-SAR in tandem mode are the excellent example of short temporal resolution. In wide range of contexts, TanDEM-X and TerraSAR-X are imaging the terrain below them simultaneously, from different angles. These images are processed into precise elevation maps with a 12 m resolution and any vertical accuracy better than 2 m [1, 3, 15, 24, 31, 38].

Additional, Gens [12] reported the time difference for two data acquisitions is a second source of decorrelation. Indeed, the time differences while compare data sets with a similar baseline length acquired one and 35 days apart suggests only the temporal component of the decorrelation. Therefore, Marghany [20] stated that the loss of coherence in the same repeat cycle in data acquisition is most likely because of baseline decorrelation and dense vegetation covers in such a tropical as Malaysia. According to Roa et al. [7], uncertainties could arise in DEM [14] because of limitation InSAR repeat passes [3, 8, 15, 21, 24]. A constant phase difference during the two images caused by the horizontally homogeneous atmosphere was over the length scale of an interferogram and vertically over that of the topography. The atmosphere, however, is laterally heterogeneous on length scales both larger and smaller than typical deformation signals [9, 17].

Journal of Advanced Research in Materials Science
ISSN (online): 2289-7992 | Vol. 4, No.1. Pages 31-46, 2015

Recently, Pepe [35] stated that DinSAR has recently applied with success to investigate the temporal evolution of the detected deformation phenomena through the generation of displacement time-series. In this context, two main categories of advanced DInSAR techniques for deformation time-series generation have been proposed in literature, often referred to as Persistent Scatterers (PS); and Small Baseline (SB) techniques, respectively. The PS algorithms select all the interferometric data pairs with reference to a single common master image, without any constraint on the temporal and spatial separation (baseline) among the orbits.

1.1 Phase Unwrapping

Phase unwrapping is a key step in extracting digital elevation models (DEMs) from interferometric synthetic aperture radar (InSAR) data. Thus the measured phases are wrapped in the interval (2 π, π], and phase unwrapping is a necessary step to recover the original full phase value [4]. In particular, phase unwrapping algorithms can be classified into two categories: (i) the path-following method; and the (ii) minimum-norm approach. The Goldstein's method is a classic path-following phase unwrapping method which searches for residues in the phase image and places branch cuts between nearby residues. In this way it removes the integration path dependency when unwrapping the phase image. The phase difference integration starts from the top left corner of the image and unwraps the phases with the assumption that adjacent pixels have phase differences within the range $[-\pi, \pi)$. Also the unwrapping path needs to integrate around branch cuts in order to remove the path dependency. However, when the branch cuts are placed in the wrong location, the unwrapping result can be incorrect [4].

The minimum-norm methods are generally iterative and usually need more computation time than the path-following integration methods. Flynn's method [35] tries to minimize the discontinuity of the phase image. The algorithm finds the path that can form the loop of discontinuity and removes the discontinuity by adding or removing 2π on the phase values within the loop region. The process is performed iteratively until no more discontinuity loops are found. A quality map can also be applied to guide the discontinuity placement. The PCG method treats unwrapping as a weighted least-squares problem. It unwraps the phase image by solving the partial differential equation iteratively. Conjugate gradient can be used to improve convergence. The weights are used to select high-quality nodes and mask out the corrupt region of the phase map. The comparison for using different two-dimensional unwrapping methods on MRE phase image block will be illustrated in more detail [30].

In proportion to Hussien et al., [28] [29],the central idea of the quality-guided path following method is to unwrap along a path starting with the highest quality pixel where little unwrapping is required to the most ambiguous areas where the phases of adjacent better quality pixels can be used to inform the unwrapping. The quality map can be a correlation map, phase derivative variance map, etc. When a correlation map is not available, the phase derivative variance map is generally used. On the word of Yang et al.[12], the phase estimation is a major challenge to determine more accurate DEM. This is because of the measured phase differences are given as a wrapped phase field of the principal values of a range $-\pi$ to π, thus the existence unspecified within multiples of 2 π [7]. This procedure produces phase jumps between neighboring pixels. Smooth function is used to resolve phase jump by adding or subtracting multiples of 2 π. Consequently, multichannel MAP height estimator based on a Gaussian Markov Random (GMRF) has developed by Baseline et al., [23] and Ferraiuol et al., [24] to solve the uncertainties of DEM reconstruction from InSAR

technique. They found that the multichannel MAP height estimator has managed the phase discontinuities and improved the DEM profile. Recently, Marghany [21] validated GMRF technique with a lower range of error (0.01±0.11 m) with 90% confidence intervals for DEM reconstruction using RADARSAT-1 SAR F1 mode data.

However, the two-dimensional unwrapping methods could introduce discontinuous regions when the noise is high. The resulting inconsistent baselines within a slice would produce an incorrectly unwrapped baseline. Then the one-dimensional baseline unwrapping could give incorrect results. Many of the methods apply to quality map to guide the unwrapping procedures. The quality map was defined with the quality of the edges that connects two neighboring voxels and unwrap the most reliable voxels first [29, 30]. Therefore, three-dimensional phase unwrapping approach, which considers the temporal domain and the spatial domain restrictions simultaneously [22].

1.2 Hypotheses and Objectives

In this paper, we address the question of utilization of inversion genetic algorithm (GA) as an optimization method to model the three-dimensional (3-D) of rate changes of shoreline. In this context, Marghany [22] used three-dimensional sorting reliabilities algorithm (3D-SRA) phase unwrapping for modelling volume rate changes of shoreline. However, 3D-SRA was not able to remove the artifacts in DEM due to radar shadow, layover, multi-path effects and image misregistration, and finally the signal-to –noise ratio (SNR) [11]. In fact, 3DSRA does not identify singularity loops at all. Its depends completely upon a quality measure to unwrap the phase volume. Ignoring singularity loops may cause the unwrapping path to penetrate these loops and errors may propagate in the unwrapped phase map.

The main contribution of this study is to combine Hybrid Genetic Algorithm (HGA) with three-dimensional phase unwrapping algorithm of three-dimensional best-path avoiding singularity loops (3DBPASL) algorithm with InSAR technique. Three hypotheses examined are: (i) the HGA algorithm can be used as filtering technique to reduce noise in the 3-D phase unwrapping; (ii) 3-D shoreline reconstruction can be produced using satisfactory phase unwrapping of 3DBPASL by involving HGA optimization algorithm; and (iii) high accuracy of coastline deformation rate can be simiulated by using HGA optimization algorithm.

2.0 METHODOLOGY

2.1 Data Set

The study area is located along the coast of Johor in the southern eastern part of Peninsular Malaysia. The area is approximately 20 km of Johor (Figure 1), located in the South China Sea between 1° 57´ N to 2° 15´ N and 103° 51´ E to 104° 15´ E. This coastline is exhibited a variety of geomorphologies that includes sandy beaches, rocky headlands which is broken by small river mouths. In addition, the coastaline has hilly terrain with steep slopes and deep narrow valleys. Further, the coastline is bordered with varying width of alluvial plains. Further, sand materials make up the entire of the eastern Johor shoreline. Consistent with Marghany [14][42], this area lies in an equatorial region dominated by two seasonal monsoons and two inter monsoon periods. According to Marghany [14] the maximum wave height during the northeast monsoon season is 4 m. The minimum wave height is found during the southwest monsoon which is less than 1 m [18].

Penerbit Akademia Baru

Journal of Advanced Research in Materials Science
ISSN (online): 2289-7992 | Vol. 4, No.1. Pages 31-46, 2015

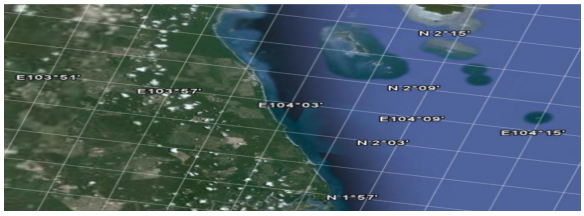

Figure 1: Location of study area

2.2 InSAR Data Processing

Three methods are involved to perform InSAR from ENVISAT SAR SAR data (i) conventional InSAR procedures; and (ii) three-dimensional phase unwrapping algorithm i.e. three-dimensional best-path avoiding singularity loops (3DBPASL) algorithm[25, 42]; and [iii] Hybrid Genetic Algorithm.

2.2.1 Conventional InSAR Method

According, Zebker et al., [4] SAR interferometry (equivalently, the InSAR technique) is a technique to extract surface physical properties by using the complex correlation coefficient of two SAR signals. The complex correlation coefficient, γ, of the two SAR observations, s_1 and s_2, is defined as:

$$\gamma = \frac{E[s_1 s_2^*]}{\sqrt{E[s_1 s_1^*]E[s_2 s_2^*]}} \quad (1)$$

where $E[]$ is the mathematical expectation (ensemble averaging) and * represents the complex conjugate [2]. Further, Hanssen [3] stated that the interferometric phase is defined as the phase of the complex correlation coefficient as:

$$\varphi = \arg\{\gamma\} = \arg\{E[s_1 s_2^*]\} \quad (2)$$

and its two dimensional map is called the interferogram. Moreover, Hanssen [3] and Zebker et al., [4] defined the coherence as the amplitude of the complex correlation coefficient which expressed as:

$$\rho = |\gamma| \quad (3)$$

and its two dimensional map is presented in the coherence image[1][3][5]. According to Zebker et al., [23] an interferogram contains the interferometric phase fringes from SAR geometry, together with those from topography and displacement of the surface. The level of coherence can give a measure of the quality of the interferogram. Initially, the InSAR techniques were mainly dedicated to topographic information retrieval from interferograms. Further development resulted in techniques to extract interferometric phase fringes from coherent block displacement of the surface [24-26]. In Marghany [22], the surface displacement can estimate using the acquisition times of two SAR data s_1 and s_2. The component of surface displacement thus, in the radar-look direction, contributes to the further interferometric phase (φ) as [9][12],

$$\phi = \frac{4\pi(\Delta R)}{\lambda} = \frac{4\pi(B_h \sin\theta - B_v \cos\theta)}{\lambda} \quad (4)$$

where ΔR is the slant range difference from satellite to target respectively at different time, θ is the look angle (19.2-26.7°) [19][42], λ is the ENVISAT ASAR wavelength Single Look Complex (SLC) which is about 5.6 cm for C- band. Therefore, B_h, B_v are horizontal and vertical baseline components [22]. Then, the phase difference $\Delta\phi$ between the two ENVISAT ASAR data positions and the pixel of target of terrain point is given by

$$\Delta\zeta = \frac{\lambda R \sin\theta}{4\pi B}\Delta\phi \quad (5)$$

Equation 5 is a function of normal base line B, and the range R. In addition, equation 5 can provide information about the heights and phase differences estimations. In fact, the estimated height of each pixel of ENVISAT ASAR data is an important task to generate a raster form of the DEM. However, this equation is required short baseline and accurate image coregisteration to acquire accurate quality of interferogram phase map.

2.2.2 DEM reconstruction using three-dimensional best-path avoiding singularity loops (3DBPASL) algorithm

Phase unwrapping in Equation 5 can be extended to three-dimensional to

$$\sum_{i,j,k} w^{x}_{i,j,k} \left|\Delta\phi^{x}_{i,j,k} - \Delta\psi^{x}_{i,j,k}\right|^{P} + \sum_{i,j,k} w^{y}_{i,j,k} \left|\Delta\phi^{y}_{i,j,k} - \Delta\psi^{y}_{i,j,k}\right|^{P} + \sum_{i,j,k} w^{z}_{i,j,k} \left|\Delta\phi^{z}_{i,j,k} - \Delta\psi^{z}_{i,j,k}\right|^{P} \quad (6)$$

where $\Delta\phi$ and $\Delta\psi$ are the unwrapped and wrapped phase differences in x,y,z, respectively, and w represents user-defined weights. The summations are carried out in both x, y and z *directions* over all i,j and k, respectively. A more advance method developed by Ghiglia *et al.*[3] is L^p-norm which uses similar methods like the two previous least square methods to solve the phase unwrapping problem. However, this method does not compute the minimum L^2-norm but the general minimum L^p-norm. In essence, by computing the minimum L^p-norm where $p\neq2$; this method can generate data dependent weight unlike the weighted least-square method. The data-dependent weights can eliminate iteratively the presence of the residues in the unwrapped solution. This method is more robust than the previous mentioned least-squares method and it is more computationally intensive [39].

Then the phase unwrapping based on the quality map can be calculated using the following equation [22, 29],

$$Q_{m,n,l} = \frac{1}{m\times n\times l} * ((\sum(\Delta\phi^{x}_{i,j,k} - \overline{\Delta\phi^{x}_{i,j,k}})^2)^{0.5} + ((\sum(\Delta\phi^{y}_{i,j,k} - \overline{\Delta\phi^{y}_{i,j,k}})^2)^{0.5} + ((\sum(\Delta\phi^{z}_{i,j,k} - \overline{\Delta\phi^{z}_{i,j,k}})^2)^{0.5}, \quad (7)$$

where $\Delta\phi^{x}, \Delta\phi^{y}$, and $\Delta\phi^{z}$ are the unwrapped-phase gradients in the x, y, and z directions, respectively. $\overline{\Delta\phi}^{x}, \overline{\Delta\phi}^{y}$, and $\overline{\Delta\phi}^{z}$ are the mean of unwrapped-phase gradient in $m\times n\times l$ cube in $\Delta\phi^{x}, \Delta\phi^{y}$, and $\Delta\phi^{z}$, respectively. $i,j,$ and k are neighbors's indices of the voxel $v_$in m, n, and l cube. Following Hussien et al., [28], the maximum gradient of the voxel v_m, n, $l\_$ can

Penerbit Akademia Baru

Journal of Advanced Research in Materials Science
ISSN (online): 2289-7992 | Vol. 4, No.1. Pages 31-46, 2015

be obtained by estimating the maximum unwrapped- phase gradient of in the *x*, *y*,or *z* directions, as described in Eq. (8).

$$X_{m.n,l} = \max\{\max\{\left|\Delta\phi^{x}_{i,j,k}\right|\}, \max\{\left|\Delta\phi^{y}_{i,j,k}\right|\}, \ \max\{\left|\Delta\phi^{z}_{i,j,k}\right|\}\} \tag{8}$$

According to Hussien et al., [28] the maximum gradient method indicates the badness rather than the goodness of the unwrapped-phase data, so the quality is calculated using the reciprocal of the unwrapped phase gradient of Equation (8.0). Further, Hussien et al., [28] [29] and Marghany [22] agreed that quality-guided phase unwrapping algorithms is function of the quality of the voxels themselves to conduct the unwrapping path and to minimize error propagation during the unwrapping procedure. In this respect, the unwrapping path algorithm is function of the quality of the edges as an intermediate stage, rather the quality of the voxels [28, 29]. Following Marghany [22] and Hussien et al., [29], the quality map of voxels can be given by

$$Q_{i,j,k} = \sqrt{H_x^{\,2}(i,j,k) + V_y^{\,2}(i,j,k) + N^{2}(i,j,k)} \tag{9}$$

where H_x, V_y, and N are the horizontal, vertical, and normal second differences, respectively [22], where,

$$H_x(i,j,k) = \left[\frac{\partial \phi_{i,j,k}{}^{x}}{[\phi_{i+1,j,k} - \phi_{i,j,k}]}\right][\Delta\phi(i-1,j,k) - \Delta\phi(i,j,k)] - \left[\frac{\partial \phi_{i,j,k}{}^{x}}{[\phi_{i+1,j,k} - \phi_{i,j,k}]}\right][\Delta\phi(i,j,k) - \Delta\phi(i+1,j,k)], \tag{10}$$

$$V_y(i,j,k) = \left[\frac{\partial \phi_{i,j,k}{}^{y}}{[\phi_{i,j+1,k} - \phi_{i,j,k}]}\right][\Delta\phi(i,j-1,k) - \Delta\phi(i,j,k)] - \left[\frac{\partial \phi_{i,j,k}{}^{y}}{[\phi_{i,j+1,k} - \phi_{i,j,k}]}\right][\phi(i,j,k) - \phi(i,j+1,k)], \tag{11}$$

$$N(i,j,k) = \left[\frac{\partial \phi_{i,j,k}{}^{z}}{[\phi_{i,j,k+1} - \phi_{i,j,k}]}\right][\Delta\phi(i,j,k-1) - \Delta\phi(i,j,k)] - \left[\frac{\partial \phi_{i,j,k}{}^{z}}{[\phi_{i,j,k+1} - \phi_{i,j,k}]}\right][\Delta\phi(i,j,k) - \Delta\phi(i,j,k+1)], \tag{12}$$

where *i*,*j*,*k* are the neighbors' indices of the voxel in 3 x 3 x 3 cube, and $\frac{\partial \phi_{i,j,k}{}^{z}}{[\phi_{i,j,k+1} - \phi_{i,j,k}]}$ defines a uwrapping operator that unwraps all values of its argument in the range $[-\pi, \pi]$. This can be done by adding or subtracting an integer number of 2π rad to its argument [22, 25, 26, 29]. Equations 10.0 to 12.0 are represented 3-D array of the unwrapped-phase gradients $\partial\phi^{x}, \partial\phi^{y}, \partial\phi^{z}$ and each has the same dimensions as the uwrapped-phase volume. In addition, the maximum phase gradient measures the magnitude of the largest phase gradient that is, partial derivative or wrapped the phase difference in a *v***v***v* volumes [29].

The unwrapping path is performed based on equation 9 where entirely the edges are stored in a 3D array and sorted with their edge quality values [26]. Further, unwrapping a voxel or a group of voxels concerning another group may require the addition or subtraction of multiples of 2π [25]. In this regard, the quality of each edge of phase unwrapping is a function of the connection of two voxels in 3-D cartesian axis e.g., *x*, *y*, *z*. Starting to optimize the unwrapping path from high quality voxels to bad quality voxels [28] by using

Journal of Advanced Research in Materials Science
ISSN (online): 2289-7992 | Vol. 4, No.1. Pages 31-46, 2015

Hybrid Genetic Algorithm (HGA). Indeed, the 3D best-path which is avoiding singularity loops (3DBPASL) algorithm may not be the shortest when the residues are dense as the isolated districts enclosed by the branch cuts can easily appear. Searching for the shortest path in the path-following algorithm is in fact an optimization problem. Several optimization approaches, such as genetic algorithms have been applied to 2-D phase unwrapping. Therefore, Hybrid Genetic Algorithm (HGA) has numerous advantages, for instance, global searching, robustness, parallelism. Further, it can be implemented with other algorithm.

2.2.3 Hybrid Genetic Algorithm

Following Karout [39], the HGA algorithm relies on estimating the parameters of an n^{th} order-polynomial to approximate the unwrapped surface solution from the wrapped phase data. The coefficients of the polynomial that best unwrap the wrapped phase map are obtained by intial solution of GA algorithm to avoid long time to converge to the global optimum solution. In this context, GA minimizes minimum 3DBPASL and $Q_{i,j,k}$ errors between the gradient of the polynomial unwrapped surface solution and the gradient of the orginal wrapped phase map. On other words, more precision and lower minimum 3DBPASL and $Q_{i,j,k}$ errors are achieved by increasing the order of the polynomial. This proposed algorithm is mainly applicable to adjoining phase distributions (albeit with gaps). Any optimisation problem using a GA requires the problem to be coded into GA syntax form, which is the chromosome form. In this problem, the chromosome consists of a number of genes where every gene correspond to a coefficient in the n^{th}-order surface fitting polynomial as described into equation (13) .

$$f := n \rightarrow \sum_{k=0}^{n} \sum_{j=0}^{n} \sum_{i=0}^{n} a_{i,j,k} \Delta \phi^{x}_{i,j,k} \Delta \phi^{y}_{i,j,k} \Delta \phi^{z}_{i,j,k} \tag{13}$$

where $a[0....n]$ are the parameter coefficients which are retrieved by the genetic algorithm to approximated the unwrapped phase that can achieve the minimum 3DBPASL and $Q_{i,j,k}$ errors. Further, i,j and k are indices of the pixel location in the unwrapped phase respectively, n is the number of coefficients.

2.2.3.1 Initial Solution and Population

The initial population is generated by creating an initial solution using one of the Quality guided phase unwrapping algorithm (BPASL algorithm) [29]. Following Karout [39], the initial solution is approximated using a 'polynomial Surface-fitting weighted least-square multiple regression' method. The intial population is then generated based on the initial solution. In doning so, every a_g in each chromosome in the population, a small number relying on the accuracy of the gene that is added or subtracted to the value of the gene as given by [39],

$$a_g = a_g + (\pm 1)\{10^{[\log(a_g)+\Re]}\} \tag{14}$$

where a_g is the coefficient parameter stored in gene g, and $\Re$ is a random number generated between the values.

Penerbit Akademia Baru

Journal of Advanced Research in Materials Science
ISSN (online): 2289-7992 | Vol. 4, No.1. Pages 31-46, 2015

2.2.3.2 Record Pareto Optimal Solutions

Calculate the objective values of chromosomes in the population and record the Pareto optimal solutions.

Definition: Pareto Optimal Solutions

Let $x_0, x_1, x_2 \in F$, and F is a feasible region. And x_0 is called the Pareto optimal solution in the minimization problem if the following conditions are satisfied.

1. If $f(x_1)$ is said to be partially greater than $f(x_2)$, i.e. $f_i(x_1) \geq f_i(x_2), \forall\, i = 1,2,...,n$ and $f_i(x_1) > f_i(x_2), \exists\, i = 1,2,...,n$, (15)
   Then x_1 is said to be dominated by x_2.
2. If there is no $x \in F$ s.t. x dominates x_0, then x_0 is the Pareto optimal solutions.

2.2.3.3 Fitness Evaluation

In this step, the quality of the solution is evaluted at every generation to determine the global optimum solution to the parameter estimation phase unwrapping problem. Therefore, the genes of a chosen chromosomes are substituted as coeficients in equation 15 to evaluate the approximated phase value at coordinate (*i*, *j*, *k*). Then,the obtained phase is subtracted from the contiguous pixel approximated phase value to reteieve the approximated unwrapped phase solution gradient. It is then subtracted from the gradient of the wrapped phase in the *i*, *j*, and *k* direction [29,39].

2.2.3.4 Crossover and Mutation

Following Haupt and Haupt [40], the two point greedy continuous crossover are implemented in crossover operator. Therefore, crossover is less problem than the mutation operator. Thus, Mutation operator concerns deliberate changes to a gene at random, to keep variation in genes and to increase the probability of not falling into a local minimum solution [39]. It involves exploring the search space for new better solutions. This proposed operator uses a greedy technique which ensures only the best fit chromosome is allowed to propagate to the next generation.

2.2.3.5 Phase Matching

The accurate 3-D phase unwrapping [29] is obtained by phase matching algorithm proposed by Schwarz [42]. According to Schwarz [42], phase matching algorithm is matched the phase of wrapped phase with unwrapped phase by the given equation

$$\psi_{i,j,k} = \Delta\phi_{i,j,k} + 2\pi\rho\left[\frac{1}{2\pi}\left(\Delta\hat{\phi}_{i,j,k} - \Delta\phi_{i,j,k}\right)\right] \tag{16}$$

where $\psi_{i,j,k}$ is the phase matched unwrapped phase, *i,j,*and *k* are the pixel positions in the quality phase map, $\Delta\phi_{i,j,k}$ is the given wrapped phase, $\Delta\hat{\phi}_{i,j,k}$ is the approximated unwrapped phase, $\rho[.]$ is a rounding function which is defined by $\rho[t] = \lfloor t + 1/2 \rfloor$ for $t \geq 0$ and $\rho[t] = \lfloor t - 1/2 \rfloor$ for $t < 0$ and are *i,j,*and *k* the pixel positions in *x* and *y,z* directions, respectively[39].

Penerbit Akademia Baru

Journal of Advanced Research in Materials Science
ISSN (online): 2289-7992 | Vol. 4, No.1. Pages 31-46, 2015

3.0 RESULTS AND DISCUSSION

Figure 2 shows the coherence map of the ENVISAT ASAR data. It is interesting to find that the coherence image coincided with backscatter variation along the coastal zone. The urban zones are dominated with higher coherence of 0.8 dB as compared to vegetation and sand wet areas. On contrast, the coastal zone has lower backscatter and coherence of 0.0 dB and 0.25, respectively. Since three ENVISAT mode data acquired in wet north-east monsoon period, there is an impact of wet sand on radar signal penetration which causing weak penetration of radar signal because of dielectric. Clearly the total topographic decorrelation effects along the radar-facing slopes are dominant and highlighted as bright features of 1 over a grey background.

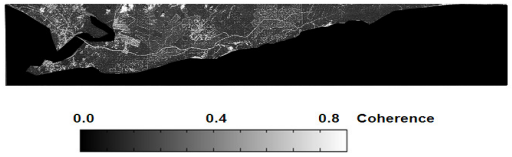

Figure 2: Coherence map of ENVISAT ASAR

It in interest to find the interferogram fringes are corresponding with the high coherence area of 1 e.g. urban and sandy areas. In contrast, vegetation area and water zone of value less than 0.2 are coincided with absent of interferogram fringe absents (Figure 3). This occurs because of decorrelation. In fact, the baseline decorrelation and temporal decorrelation make InSAR measurements unfeasible. This result is agreed with with Marghany [27, 31].

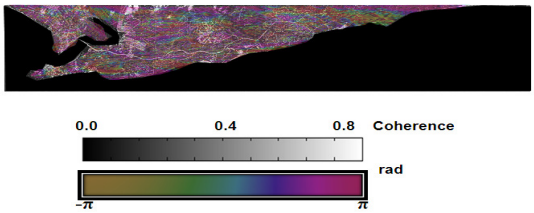

Figure 3. Combination of coherence and interferometry

Marghany [22] reported that the wet northeast monsoon period where three ASAR data were acquired, has been an impact of wet sand on a radar signal penetration which causing weak penetration of radar signal because of dielectric. Indeed, the total topographic decorrelation effects along the radar-facing slopes are dominant and highlighted as lowest coherence value of 0.2. According to Marghany [27] the micro-scale movement of the sand particles driven by the coastal hydrodynamic, and wind speed of 12 m/s during northeast monsoon period [30] could change the distribution of scatters resulting in rapid temporal decorrelation which has contributed to lowest coherence along coastline [22]. Figure 4 shows the interferometry fringes produced by using Hybrid Genetic Algorithm based on Pareto Optimal Solutions. It is interesting to find that the proposed algorithm has produced clear features detection of infrastructures. In fact, the proposed algorithm has minimized the error in interferogram cycle due the low coherence in vegetation zones and along the wet sand of coastline.

Penerbit Akademia Baru

Journal of Advanced Research in Materials Science
ISSN (online): 2289-7992 | Vol. 4, No.1. Pages 31-46, 2015

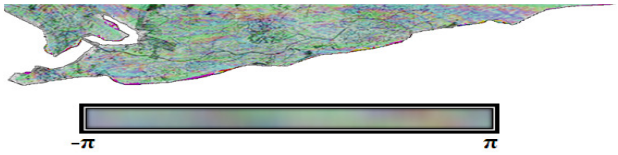

Figure 4: Interferometry produced by Hybird Genetic Algorithm

Figure 5 shows the interferogram fringes produced by using the combination of three-dimensional best-path avoiding singularity loops (3DBPASL) algorithm and HGA algorithm. Clearly, the proposed algorithm for 3D phase unwrapping produced vibrant fringe cycles which indicate critical erosion of -3.5 m/year. This study confirms the work done by Hussein et al.,[28]. In fact, the 3DBPASL algorithm acquires an optimal unwrapping path, whereas it is also taking into account the effect of singularity loops. In addition, zero-weighted edge is used zero-weighted edges to adjust the optimal path and avoid these singularity loops. In line with Hussien et al., [28],the 3DBPASL not only identifies these singularity loops, but it also calculates the quality of each voxel to ensure that the most reliable voxels are unwrapped first and thus the effects of singularity loop ambiguities are minimized or removed entirely. Therefore, the combination of 3DBPASL for phase unwrapping with hybrid Genetic algorithm produced more precisely fringe cycle. In this regard, hybrid Genetic algorithm matches the phase of the wrapped phase with approximated unwrapped phase to establish the best representation of the unwrapped phase. Figure 5 shows the 3-D volume of coastline deformation produced by inversing of HGA algorithm along the coastal waters of Johor, Malaysia. The erosion event is confirmed by volume rate changes of -3000 m^3/year. According to Karout [39], a genetic algorithm is used to estimate the coefficient of an n^{th}-order polynomial that best approximates the unwrapped phase map which minimizes the difference between the unwrapped phase gradient and the wrapped phase gradient. The genetic algorithm is uses an initial solution to speed convergence. The initial solution is achieved by unwrapping using a simple unwrapping algorithm and estimating the parameters of the polynomial using weighted least squares multiple regression.

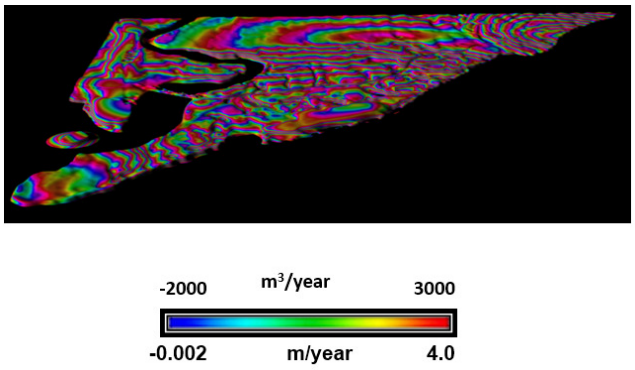

Figure 5: 3-D volume of coastline deformation

Table 1 shows the statistical comparison between the simulated DEM from the InSAR, real ground measurements and with using Hybrid Genetic Algorithm for three-dimensional best-

Journal of Advanced Research in Materials Science
ISSN (online): 2289-7992 | Vol. 4, No.1. Pages 31-46, 2015

path avoiding singularity loops (3DBPASL). This table represents the bias (averages mean the standard error, 90 and 95% confidence intervals, respectively.

Table 1: Statistical Comparison between InSAR and Hybrid Genetic Algorithm for three-dimensional best-path avoiding singularity loops (3DBPASL)

Statistical parameters	**InSAR techniques**			
	InSAR		**Hybrid Genetic Algorithm (GHA) for 3DBPASL**	
Bias	3.3		-0.06	
Standard error of the mean	2.2		0.03	
	Lower	**Upper**	**Lower**	**Upper**
90%	2.3	3.8	0.03	0.13
90% confidence interval	1.3	3.2	0.03	0.21

Evidently, the InSAR using Hybrid Genetic Algorithm for three-dimensional best-path avoiding singularity loops (3DBPASL) algorithm has bias of -0.06 m, lower than ground measurements and the InSAR method. Therefore, Hybrid Genetic Algorithm for three-dimensional best-path avoiding singularity loops (3DBPASL) has a standard error of mean of ± 0.03 m, lower than ground measurements and the InSAR method. Overall performances of InSAR method using Hybrid Genetic Algorithm for three-dimensional best-path avoiding singularity loops (3DBPASL) algorithm is better than conventional InSAR technique which is validated by a lower range of error (0.04±0.22 m) with 90% confidence intervals.

4.0 CONCLUSSION

The paper is focused on three-dimensional (3-D) coastline deformation from interferometry synthetic aperture radar (InSAR). In doing so, conventional InSAR procedures are implemented to three repeat passes of ENVISAT ASAR data. Further, the three dimensional phase unwrapping is performed using three-dimensional best-path avoiding singularity loops (3DBPASL) algorithm. Then phase matching is implemented with 3DBPASL using Hybrid Genetic Algorithm (GHA). Further, the combination between GHA and 3DBPASL is used to eliminate the phase decorrelation impact from the interferograms. The study shows the performance of InSAR method using the Hybrid Genetic Algorithm for three-dimensional best-path avoiding singularity loops (3DBPASL) which is validated by a lower range of error (0.04±0.22 m) with 90% confidence intervals. In conclusion, integration of the GHA with 3DBPASL phase unwrapping produce accurate 3-D coastline deformation.

ACKNOWLEDGEMENT

The author would like to thank the Universiti Teknologi Malaysia and Ministry of Malaysian High Education(MOHE)for funding this project under project number R.J.130000.7809.4L140 . Further, the author would like to thank research management center (RMC) of university Teknologi Malaysia for excellent assistance and guidance.

REFERENCES

[1] D. Massonnet, K.L. Feigl, Radar interferometry and its application to changes in the earth's surface, Reviews of Geophysics 36 (1998) 441-500.

[2] R. Burgmann, P.A. Rosen, E.J. Fielding, Synthetic aperture radar interferometry to measure Earth's surface topography and its deformation, Annual Review of Earth and Planetary Sciences 28 (2000) 169-209.

[3] R.F. Hanssen, Radar Interferometry: Data Interpretation and Error Analysis, Kluwer Academic, Dordrecht, Boston, 2001.

[4] H.A. Zebker, P.A. Rosen, S. Hensley, Atmospheric effects in inteferometric synthetic aperture radar surface deformation and topographic maps. Journal of Geophysical Research 102 (1997) 7547-7563.

[5] L. Hai, W. Renbiao, Robust interferometric phase estimation in InSAR via joint subspace projection, in: I. Padron (Ed.), Recent Interferometry Applications in Topography and Astronomy, InTech - Open Access Publisher, University Campus STeP Ri, Croatia, 2012, pp. 111-132.

[6] J. Askne, M. Santoro, G. Smith, J.E.S. Fransson, Multitemporal repeat-pass SAR interferometry of boreal forests, IEEE Transactions on Geoscience and Remote Sensing 41 (2003) 1540-1550.

[7] V. Nizalapur, R. Madugundu, J.C. Shekhar, Coherence-based land cover classification in forested areas of Chattisgarh, Central India, using environmental satellite-advanced synthetic aperture radar data, Journal of Applied Remote Sensing 5 (2011) 059501-1-059501-6.

[8] K.S. Rao, H.K. Al Jassar, S. Phalke, Y.S. Rao, J. P. Muller, Z. Li, A study on the applicability of repeat pass SAR interferometry for generating DEMs over several Indian test sites, International Journal of Remote Sensing 27 (2006) 595-616.

[9] K.S. Rao, H.K. Al Jassar, Error analysis in the digital elevation model of Kuwait desert derived from repeat pass synthetic aperture radar interferometry, Journal of Applied Remote Sensing 4 (2010) 1-24.

[10] H. Lee, Interferometric synthetic aperture radar coherence imagery for land surface change detection, Ph.D thesis, University of London, 2001.

[11] X. Luo, F. Huang, G. Liu, Extraction co-seismic deformation of bam earthquake with differential SAR interferometry, Journal of New Zealand Institute of Surveyors 296 (2006) 20-23.

[12] J. Yang, T. Xiong, Y. Peng, A fuzzy approach to filtering interferometric SAR data, International Journal of Remote Sensing 28 (2007) 1375-1382.

[13] R. Gens, The influence of input parameters on SAR interferometric processing and its implication on the calibration of SAR interferometric data, International Journal of Remote Sensing 2 (2000) 11767-1771.

[14] A.M. Anile, B. Falcidieno, G. Gallo, M. Spagnuolo, S. Spinello, Modeling uncertain data with fuzzy B-splines, Fuzzy Sets and Systems 113 (2000) 397-410.

[15] M. Marghany, Simulation of 3-D coastal spit geomorphology using differential synthetic aperture interferometry (DInSAR), in: I. Padron (Ed.), Recent Interferometry Applications in Topography and Astronomy. Croatia: InTech - Open Access Publisher, 2012, pp. 83-94.

[16] U. Spangnolini, 2-D phase unwrapping and instantaneous frequency estimation, IEEE Transactions on Geoscience and Remote Sensing 33 (1995) 579-589.

[17] G.W. Davidson, R. Bamler, Multiresolution phase unwrapping for SAR interferometry, IEEE Transactions on Geoscience and Remote Sensing 37 (1999) 163-174.

[18] ENVISAT, ENVISAT application [online] Available from http:\www.esa.int [Accessed 2 Febraury 2014].

[19] M. Marghany, DInSAR technique for three-dimensional coastal spit simulation from radarsat-1 fine mode data, Acta Geophysica 61 (2013) 478-493.

[20] M. Marghany, Three dimensional Coastal geomorphology deformation modelling using differential synthetic aperture interferometry, Verlag Der Zeitschrift fur Naturforschung 67a (2012) 419-420.

[21] M. Marghany, DEM reconstruction of coastal geomorphology from DINSAR. In B. Murgante, O. Gervasi, S. Misra, N. Nedjah, A.M.A.C. Rocha, D. Taniar, B.O. Apduhan, (Eds.), Lecture Notes in Computer Science (ICCSA 2012), Part III, LNCS 7335, 2012, pp. 435-446.

[22] M. Marghany, Three dimensional coastline deformation from insar envisat satellite data, in: B. Murgante, S. Misra, M. Carlini, C.M. Torre, H.-Q. Nguyen, D. Taniar, B.O. Apduhan, O. Gervasi (Eds.), Computational Science and Its Applications – ICCSA 2013, 7972, 2013, pp. 599-610.

[23] H.Z. Zebker, C.L. Werner, P.A. Rosen, S. Hensley, Accuracy of topographic maps derived from ERS-1 interferometric radar, IEEE Geoscience and Remote Sensing Letters 2 (1994) 823-836.

[24] F. Baselice, G. Ferraioli, V. Pascazio, DEM reconstruction in layover areas from SAR and auxiliary input data, IEEE Geoscience and Remote Sensing Letters 6 (2009) 253-257.

[25] G. Ferraiuolo, V. Pascazio, G. Schirinzi, Maximum a posteriori estimation of height profiles in InSAR imaging, IEEE Geoscience and Remote Sensing Letters 1 (2) (2004) 66-70.

[26] G. Ferraiuolo, F. Meglio, V. Pascazio, G. Schirinzi, DEM reconstruction accuracy in multichannel SAR interferometry, IEEE Transactions on Geoscience and Remote Sensing 47 (2009) 191-201.

[27] A. Ferretti, C. Prati, F. Rocca, Multibaseline phase unwrapping for InSAR topography estimation, Il Nuovo Cimento C 24 (2001) 159-176.

[28] H. Abdul-Rahman, M. Arevalillo-Herráez, M. Gdeisat, D. Burton, M. Lalor, F. Lilley, C. Moore, D. Sheltraw, M. Qudeisat, Robust three-dimensional best-path phase-unwrapping algorithm that avoids singularity loops, Applied Optics 23 (2009) 4582-4596.

[29] H.S. Abdul-Rahman, M.A. Gdeisat, D.R. Burton, M.J. Lalor, F. Lilley, C.J. Moore, Fast and robust three-dimensional best bath phase unwrapping algorithm, Applied Optics 46 (2007) 6623-6635.

[30] X. Wei, I. Cumming, A region-growing algorithm for insar phase unwrapping. IEEE Transactions on Geoscience and Remote Sensing 37 (1) (1999) 124-134.

[31] M.A. Costantini, Novel phase unwrapping method based on network programming, IEEE Transactions on Geoscience and Remote Sensing 36 (3) (1998) 813-831.

[32] R.M. Goldstein, H.A. Zebker, C.L. Werner, Satellite radar interferometry: two dimensional phase unwrapping, Radio Science 23 (4) (1988) 713-720.

[33] B. Ireneusz, M.P. Stewart, P.M. Kampes, P. Zbigniew, L. Peter, A modification to the goldstein radar interferogram filter, IEEE Transactions on Geoscience and Remote Sensing 41 (9) (2003) 2114-2118.

[34] W. Nan, F. Da-Zheng, L. Junxia, A locally adaptive filter of interferometric phase images, IEEE Geoscience and Remote Sensing Letters 3 (1) (2006) 73-77.

[35] Y. Qifeng, X. Yang, S. Fu, X.-L. Liu, X.-Y. Sun, An adaptive contoured window filter for interferometric synthetic aperture radar, IEEE Geoscience and Remote Sensing Letters 4 (1) (2007) 23-26.

[36] M. Marghany, Simulation of 3-D coastal spit geomorphology using differential synthetic aperture interferometry (DInSAR), in: I. Padron (Ed.), Recent Interferometry Applications in Topography and Astronomy, InTech - Open Access Publisher, University Campus STeP Ri, Croatia, 2012, pp. 83-94.

[37] A. Pepe, Advanced multitemporal phase unwrapping techniques for dinsar analyses, in: I. Padron (Ed.), Recent Interferometry Applications in Topography and Astronomy, InTech - Open Access Publisher, University Campus STeP Ri, Croatia, 2012, pp. 57-82.

[38] A. Moreira, G. Krieger, I. Hajnsek, D. Hounam, M. Werner, S. Riegger, E. Settelmeyer, TanDEM-X: A TerraSAR-X Ad on Satellite for Single Pass SAR Interferometry', Proceedings IGARSS'05, Anchorage, Alaska, vol. II, (2004) pp. 1000-1003.

[39] S. Karout, Two-Dimensional Phase Unwrapping, Ph.D Theses, Liverpool John Moores University, 2007.

Journal of Advanced Research in Materials Science
ISSN (online): 2289-7992 | Vol. 4, No.1. Pages 31-46, 2015

[40] R.L. Haupt, S.E. Haupt, Practical Genetic Algorithms, John-Wiley & Sons, 2004.

[41] S.S. Saravana, S.G. Ponnanbalam, C.A. Rajendran, Multiobjective genetic algorithm for scheduling a flexible manufacturing system, International Journal of Advanced Manufacturing Technology, 22 (2003) 229-236.

[42] O. Schwarz, Hybrid Phase Unwrapping in Laser Speckle Interferometry with Overlapping Windows, Shaker Verlag, Aachen, 2004.

[43] H. Zhong, H Tang, S. Zhang, M. Chen, An improved quality-guidedphase-unwrapping algorithm based on priority queue, IEEE Geoscience and Remote Sensing Letters 8 (2) (2011) 364-368.

[44] D.C. Ghiglia, M.D. Pritt, Two-Dimensional Phase Unwrapping: Theory, Algorithm, and Software, New York, NY, USA: Wiley, 1998.

[45] D. Gao, F. Yin, Mask cut optimization in two-dimensional phase unwrapping, IEEE Geoscience and Remote Sensing Letters 9 (3) (2012) 338-342.